

AMS Trigger Efficiency During the STS-91 Mission

Diego Casadei¹

Dipartimento di Fisica, Università di Bologna, via Imerio 46, I-40126 Bologna, Italy

(Updated on Sep. 2002)

ABSTRACT

This is a preliminary report on the AMS trigger efficiency during the STS-91 mission, showing the charge and rigidity possible dependence of the different trigger levels and conditions.

Subject headings: AMS: trigger efficiency, acceptance.

Contents

1	Introduction	1
2	The AMS trigger	2
3	AMS efficiency	3
3.1	Trigger efficiency	3
3.2	Total efficiency	3
3.3	Unfolding	3
4	Binning	3
4.1	Binning in β	4
4.2	Rigidity binning	4
4.3	Charge binning	4
4.4	Solid angle binning	4
5	Analysis of prescaled events	5
5.1	Good events distribution	5
5.2	Anticoincidence veto	5
5.3	Level 3 trigger	6
5.4	Reconstructed events	6
6	Conclusion	10

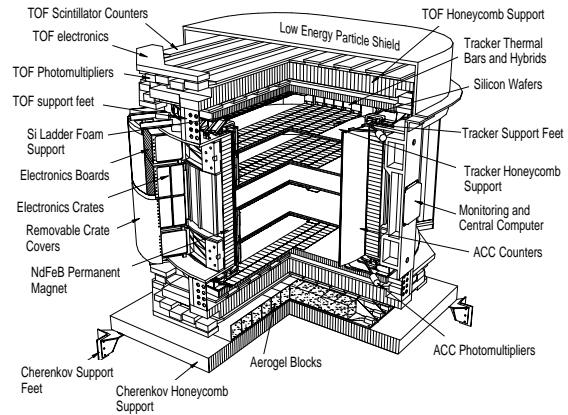


Figure 1. The AMS detector for the STS-91 mission.

1. Introduction

The *Alpha Magnetic Spectrometer* (AMS) [1] is a particle detector that will be installed on the International Space Station during the year 2002, and will take data for at least three years.

During the NASA STS-91 mission (2-12 June 1998), aboard of the shuttle Discovery, in its test flight, AMS collected data for about 180 hours. Figure 1 shows the detector, consisting of a permanent Ne-Fe-B magnet enclosing four of the six silicon tracker planes and the anticoincidence scintillator counters, four layers of scintillator counters that constitute the time of flight (TOF) system, and a threshold aerogel Čerenkov detector.

¹Diego.Casadei@bo.infn.it

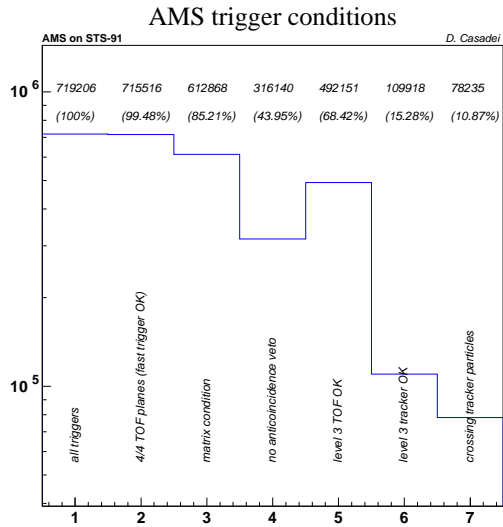


Figure 2. Trigger cuts on prescaled data.

In order to verify the trigger efficiency, about the 0.1% of the events was taken using a minimal trigger logic: only the signal from the four TOF planes was requested to acquire the events. This paper shows the results of the analysis of those “prescaled” data.

2. The AMS trigger

AMS has two levels of trigger logic. The “first level” processes only the scintillators data in a very fast way, then the tracker information is used. The tracker response is about two order of magnitude slower than the scintillators one, hence there is enough time to do a more complex on-fly analysis. The second level is then called “third level trigger”. Figure 2 shows the impact of the different trigger conditions² on the prescaled data.

In order the event to be acquired, the first condition (called “fast trigger”) is the presence of a signal in at least three of the four TOF planes. If within the next 200 ns one among the other conditions is not satisfied, the event is discarded and AMS waits for another fast trigger. Figure 2 shows that about a 0.5% of the fast triggers is due to noise (compare the second to the first bin in the histogram).

Each TOF plane consists of 14 scintillator counters, read by 3 photomultipliers at each side. The fast

²Each bin is the result of the application of only one trigger condition.

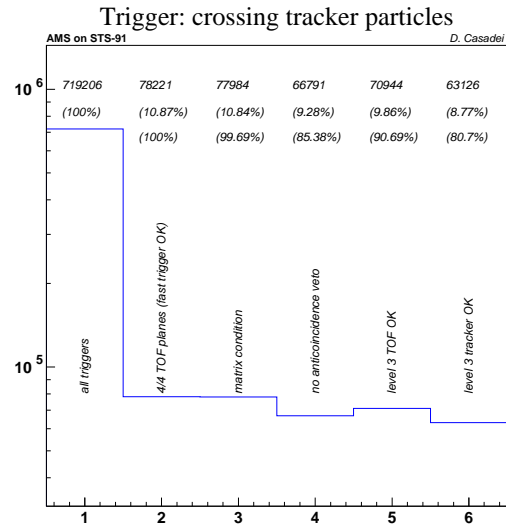


Figure 3. Trigger cuts for reconstructed prescaled events.

trigger requires at least a signal from one side of one counter in each plane. The coincidence of both sides of the counters used by the fast trigger and the existence of only one hit counter in the first and last planes, will be checked by the third level trigger. This consistency test is represented by the fifth bin of figure 2: it discards about a 30% of the fast triggers.

The next first level trigger condition, called “matrix condition”, simply discards all the tracks that don’t intersect the tracker, that has a geometrical acceptance of about $0.16 \text{ m}^2 \text{ sr}$. Only a 85% of the fast triggers survives to this cut.

The last condition at the first level trigger is the absence of signal from the anticoincidence counters (44% of the fast triggers).

The third level trigger, in addition to the consistency of the TOF counters data, requires that the position given by the TOF counters and the position extrapolated from the tracker differ of less than 6 cm (sixth bin of figure 2), leaving about 15% of the triggers.

A triggered event can still be not reconstructed as a particle track or a cluster of tracks, and this happens with the 89% of fast triggers.

If we consider only the reconstructed prescaled events (10.87% of the fast triggers), we can still see the influence of the different trigger conditions (figure 3). The only interesting thing is that the matrix condition

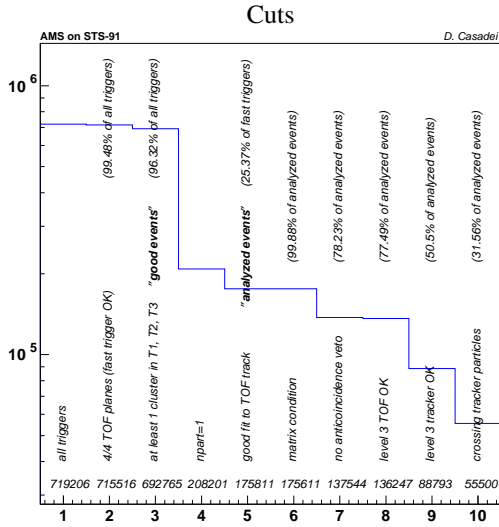


Figure 4. Trigger and analysis cuts on prescaled data.

discards a 0.3% of these events.

Figure 4 shows all the cuts applied during the analysis of prescaled data. In order to be able to find the possible charge, rigidity or direction influence on the trigger conditions, we had to require at least one cluster in the first three TOF planes (bin 3 of figure 4, “good events”), and the existence of a unique (bin 4) and well fitted track (bin 5). This allows us to do a complete analysis of the events, using only the TOF system [4], while leaving only a 25.4% (fifth bin) of the original triggers, that we will call “analyzed events”. The first condition (at least 1 cluster in planes T1, T2 and T3) leaves the $(96 \pm 1)\%$ of all the real incident particles [5].

The different trigger conditions were applied to this analysis sample in succession: first the “matrix”, then the anticoincidence veto, and so on (see figure 4). The “level 3 TOF” condition, essentially is the same thing as requiring at least 1 cluster in planes T1, T2 and T3, and only one fitted track (“npart=1”), hence it cuts away only the 0.7% of the selected events.

3. AMS efficiency

3.1. Trigger efficiency

Let N_{TOF} be the number of analyzed good events (bin 5 of figure 4). Because the good events are (with $\varepsilon_{TOF} = (96 \pm 1)\%$ efficiency [5]) those related to real

particles traversing the TOF, we will normalize to this number.

Let $N_m = N_m(R, Z; \theta, \phi)$ be the number of events satisfying the matrix condition (bin 6) as function of the incident particle rigidity R , charge Z , and incident direction; let $N_a = N_a(R, Z; \theta, \phi)$ be the number of the events without the anticoincidence counters veto (bin 7), and $N_3 = N_3(R, Z; \theta, \phi)$ the number of events left by the third level trigger conditions (bin 9).

We call *trigger efficiency* the function:

$$\varepsilon_t(R, Z; \theta, \phi) = \frac{N_3(R, Z; \theta, \phi)}{N_{TOF}} \varepsilon_{TOF}. \quad (1)$$

3.2. Total efficiency

If $N_r = N_r(R, Z; \theta, \phi)$ is the number of reconstructed events, the *reconstruction efficiency* is defined as:

$$\varepsilon_r(R, Z; \theta, \phi) = \frac{N_r(R, Z; \theta, \phi)}{N_3(R, Z; \theta, \phi)}, \quad (2)$$

while the *total efficiency* is:

$$\varepsilon(R, Z; \theta, \phi) = \frac{N_r(R, Z; \theta, \phi)}{N_{TOF}} \varepsilon_{TOF}. \quad (3)$$

3.3. Unfolding

We are interested in the differential flux $N = N(R, Z) (\text{m}^2 \text{srsGV})^{-1}$ of the various cosmic rays nuclei. Due to the finite resolution of AMS, the number of reconstructed events is:

$$N_r(R, Z) = T \int A(R, Z; \theta, \phi) N(R, Z; \theta, \phi) d\Omega, \quad (4)$$

where T (s) is the total live time, $A(R, Z; \theta, \phi) (\text{m}^{-2})$ is the AMS response function [3], and $N_r(R, Z) (\text{GV}^{-1})$ are the measured ions fluxes.

The response function can be found only through a Monte Carlo simulation of the detector: the prescaled data analysis is actually a validation of the simulation and of the unfolding method that gives $N(R, Z)$ from $N_r(R, Z)$.

4. Binning

In order to find out the dependence from the incident particle direction, charge and rigidity, we can use only the TOF data (the only subdetector crossed by all the triggering particles). The TOF system is able to measure the particle velocity to light speed ratio β , and

also the particle charge and rigidity [4], even though with a usually worst resolution compared to that of the tracker.

In the following, the histograms showing the charge, rigidity and β distribution of cosmic rays have been normalized for the bin width, in order to get the measured differential spectra.

4.1. Binning in β

The variable $\alpha \equiv 1/\beta$ is gaussian distributed with a standard deviation $\sigma_\alpha \lesssim 0.03$ for $\beta < 0.95$ [4], then the bins width for α should be a constant k of the same order of magnitude of σ_α ($k = 2\sigma_\alpha$ for example): the left edge α_i of the bin i can be: $\alpha_i \in \{1, 1+k, 1+2k, \dots, \alpha_{\max}\}$. Then the binning in β should have variable width:

$$\beta_i \in \{1, (1+k)^{-1}, (1+2k)^{-1}, \dots, (1+nk)^{-1}, \beta_m\} \quad (5)$$

(in decreasing order).

If β_m is the minimum value for β , we must choose the maximum integer n such that $\beta_m < (1+nk)^{-1}$, that is

$$n < \frac{1 - \beta_m}{k\beta_m}. \quad (6)$$

The data show that we can take $\beta_m \approx 0.3$. We choose $k = 0.05$ (approximately $2\sigma_\alpha$) and get 45 bins of different width, with at least a population of 20 (see figure 5).

4.2. Rigidity binning

We can express the rigidity as function of $\alpha = 1/\beta$ in the following way:

$$R = \frac{pc}{Ze} = \frac{\beta\gamma mc^2}{Ze} = \frac{mc^2}{Ze\sqrt{\alpha^2 - 1}}. \quad (7)$$

If we then put $m = Am_u$, where A is the nucleus mass number and m_u is the atomic mass unit ($m_u c^2 = 931.494 \text{ MeV}$), we see that the rigidity depends only upon the mass to charge ratio and the velocity of the incident particle³:

$$R \approx 0.93 \frac{A}{Z\sqrt{\alpha^2 - 1}} \quad (\text{GV}). \quad (8)$$

³The formula (8) is not valid for pions and all the other particles with mass smaller than the proton mass.

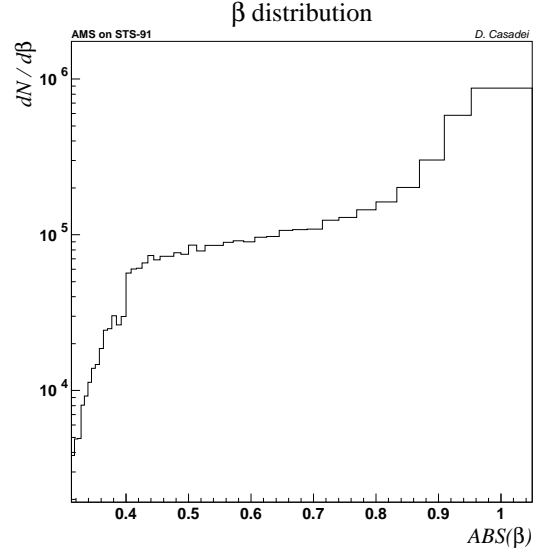


Figure 5. β distribution of prescaled data.

The (variable) width of the rigidity bins can be inferred from that of α :

$$R_i \in \left\{ \infty, \frac{m_u c^2 A/Z}{\sqrt{(1+k)^2 - 1}}, \frac{m_u c^2 A/Z}{\sqrt{(1+2k)^2 - 1}}, \dots, \frac{m_u c^2 A/Z}{\sqrt{(1+nk)^2 - 1}}, R_{\min} \right\} \quad (9)$$

where $R_{\min} = R(\beta_m) = 0.028A/Z \text{ GV}$. The A/Z ratio is about 1 for protons and about 2 for the light nuclei, thus we can use the TOF charge measurement to select the appropriate ratio.

4.3. Charge binning

While the TOF system can discriminate between charge one and greater than one at the 0.5% level [4], its charge resolution is not good for $Z > 2$. Then for this analysis a variable binning was chosen, whose limits are:

$$Z_i/e \in \{0.5, 1.5, 2.5, 5.0, 7.5, 10.0, 12.5\} \quad (10)$$

(as shown in figure 6).

4.4. Solid angle binning

The TOF system can measure the colatitude θ and the azimuth $\phi \pmod{\pi}$ angles with standard deviations $\sigma_\theta = 0.007 \text{ rad}$ and $\sigma_\phi = 0.02 \text{ rad}$ respectively [4]. The

chosen bin widths are $\Delta\theta = 0.02$ rad (about $2.9\sigma_\theta$), and $\Delta\phi = 0.05$ rad (about $2.5\sigma_\phi$).

5. Analysis of prescaled events

In this section we will show how the different trigger conditions depend upon the incident particle direction, charge and rigidity.

5.1. Good events distribution

Figure 7 shows the direction, charge and rigidity distribution of the incident particles, while figures 8 and 9 show the rigidity and incident direction for different charges.

Apart from a scale factor, the charge and rigidity distribution of the events surviving the matrix condition are the same, while there is a slightly different direction distribution for Helium nuclei, (compare figures 7 and 10), due to the pure geometrical nature of this condition. For higher charges, the number of events passing the “matrix” condition is equal to the good events number.

5.2. Anticoincidence veto

Figures 11, 12, 13 and 14 show the particles not vetoed by the anticoincidence counters as function of charge, rigidity and incident direction.

One expects that the production of secondaries and delta rays is greater for greater charges, with increasing probability to be vetoed by the anticoincidence counters, and the first three bins of figure 11 seem to confirm this idea. For the successive bins the behaviour is apparently different, but this could be simply an effect of the poor charge resolution of the TOF system. In fact, as shown in figure 15, for any ion (detected by the tracker) the TOF charge distribution has a big right tail, whose importance is particularly evident for Li and Be nuclei. The TOF system has a great probability to assign a wrong, greater charge to every particle, and this could be the cause of the strange behaviour shown in figure 11. Anyway, this argument is not conclusive.

Figure 12 shows a little suppression of particles with rigidity below $(3 \div 4)$ GV. Figure 13 shows a suppression of upward going He nuclei, compared to upward going protons. This is probably due to a greater number of secondaries produced into the greater amount of material existing under AMS. For statistical reasons (no upward $Z > 2$ events among the

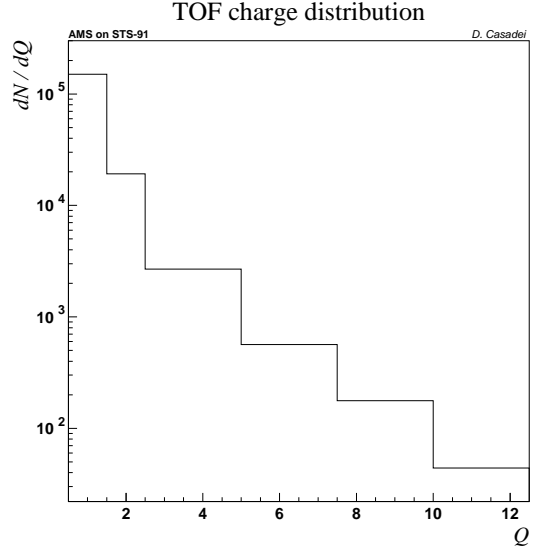


Figure 6. Charge distribution as seen by the TOF system.

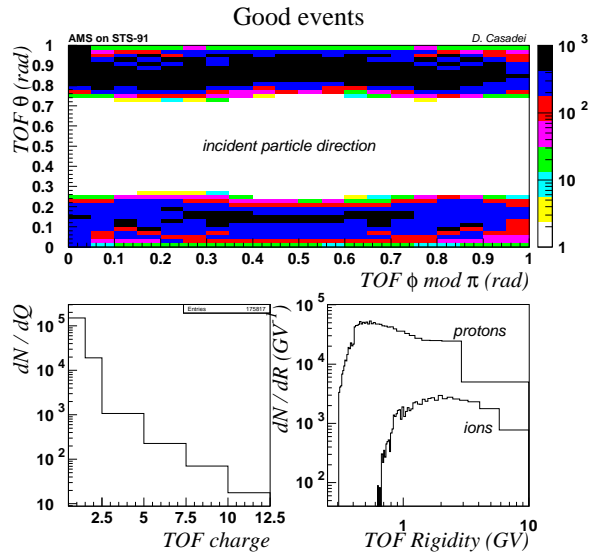


Figure 7. Good events direction, charge and rigidity.

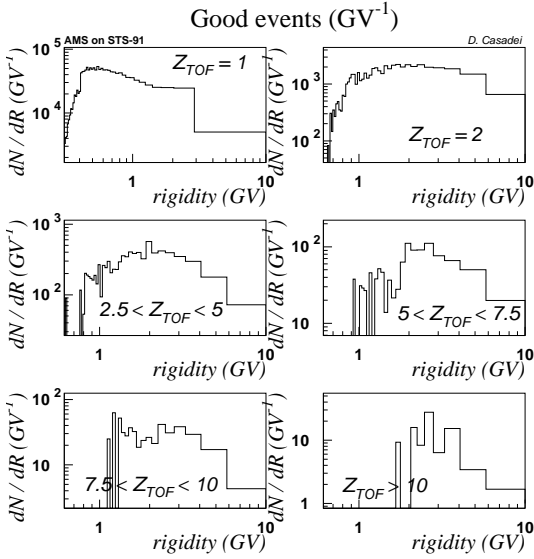


Figure 8. Good events rigidity for different charges.

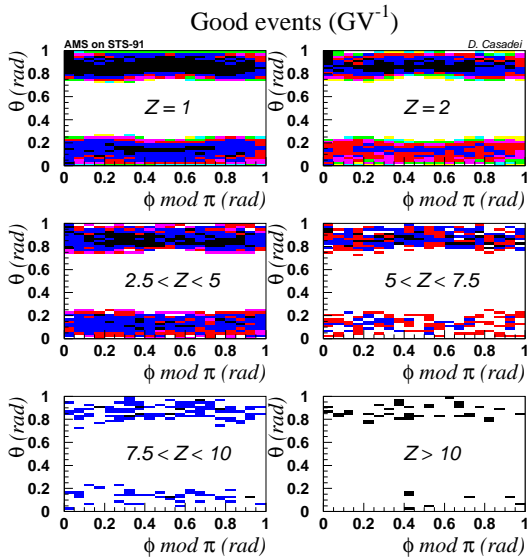


Figure 9. Good events incident direction for different charges.

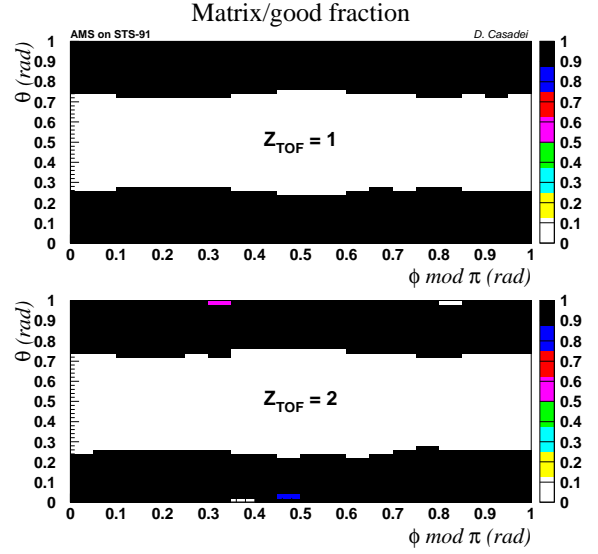


Figure 10. Matrix to good events fraction as function of the incident direction, for protons and α particles.

prescaled sample) we are not able to check this behaviour with higher charges.

5.3. Level 3 trigger

Figures 16, 17, 18 and 19 show the ratio between the events that passed the level 3 trigger to those that passed the level 1 only, as function of charge, rigidity and direction.

Figure 16 shows the same behavior of figure 11, with the exception of protons, that are cut away more strongly by the level 3 conditions.

Figure 17 has a nearly constant ratio for every charge bin, showing no rigidity dependence, and figure 18 may show slightly less events coming with $\phi \sim \pm\pi/2$ rad, that is for directions roughly laying in the (y, z) plane.

5.4. Reconstructed events

Figure 20 shows the reconstructed events charge, rigidity and direction as seen by tracker and TOF. The slightly different rigidity spectrum seen from tracker and TOF is due to their different resolution [4].

Figure 21 shows at most a weak dependence from the particle charge, while figure 22 shows a suppression of the events with $\phi \approx \pm\pi/2$, that is with a great component of the incident direction on the (y, z) plane.

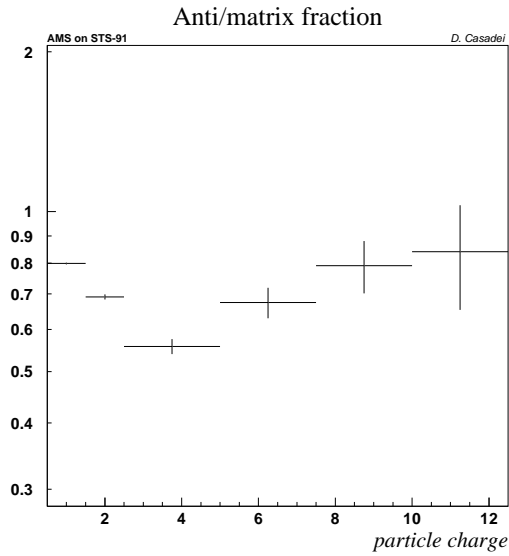


Figure 11. Ratio of particles not vetoed by anticoincidence to good events allowed by the matrix condition, as function of charge.

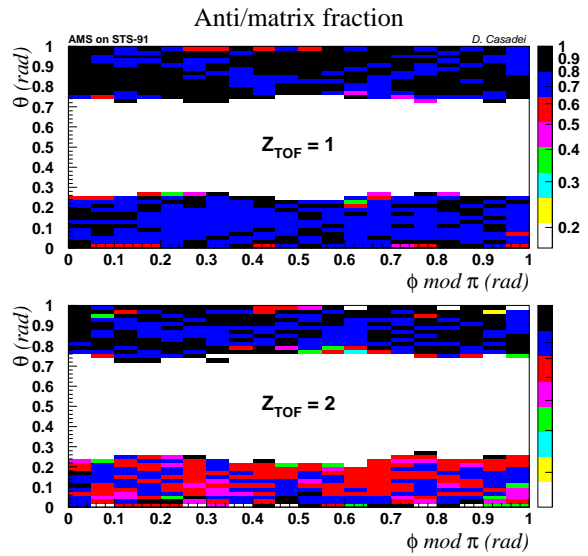


Figure 13. Ratio of particles not vetoed by anticoincidence to good events allowed by the matrix condition, as function of direction.

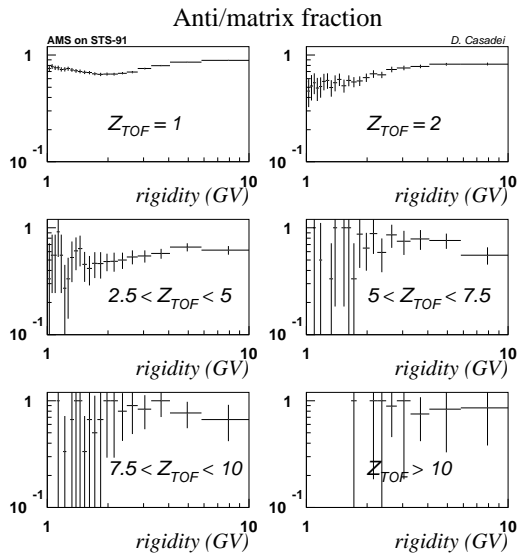


Figure 12. Ratio of particles not vetoed by anticoincidence to good events allowed by the matrix condition, as function of rigidity.

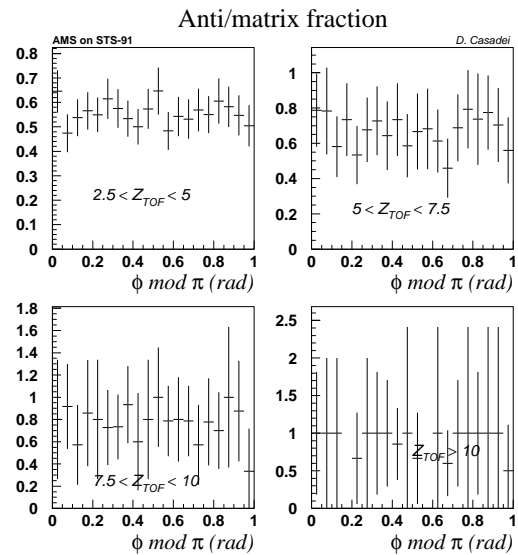


Figure 14. Ratio of particles not vetoed by anticoincidence to good events allowed by the matrix condition, as function of direction.

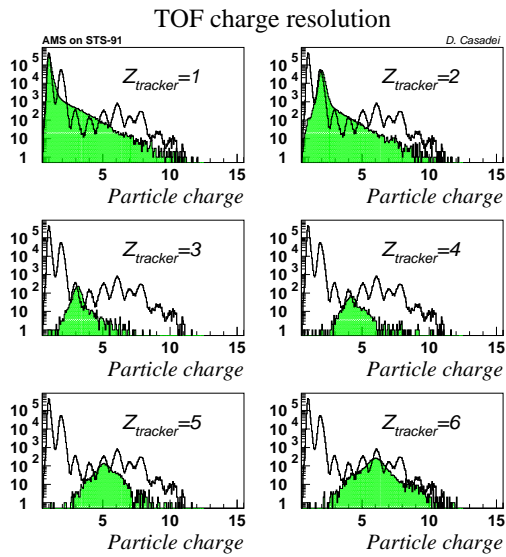


Figure 15. TOF charge distribution (shaded) of selected (with tracker) charges. The tracker distribution is shown as comparison.

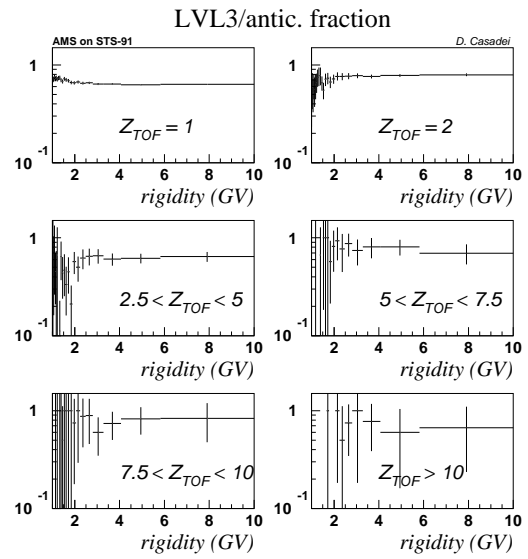


Figure 17. Level 3 to level 1 events ratio as function of rigidity.

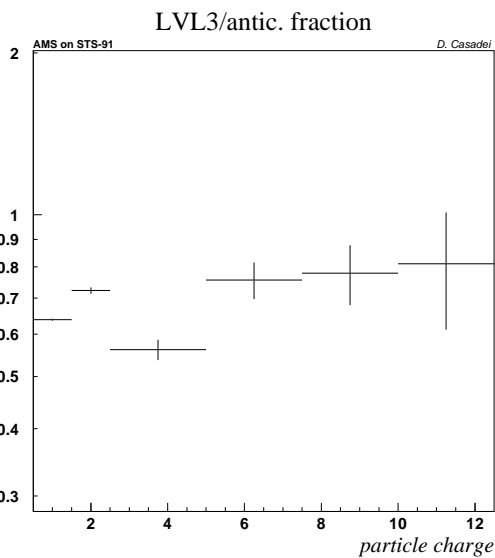


Figure 16. Level 3 to level 1 events ratio as function of charge.

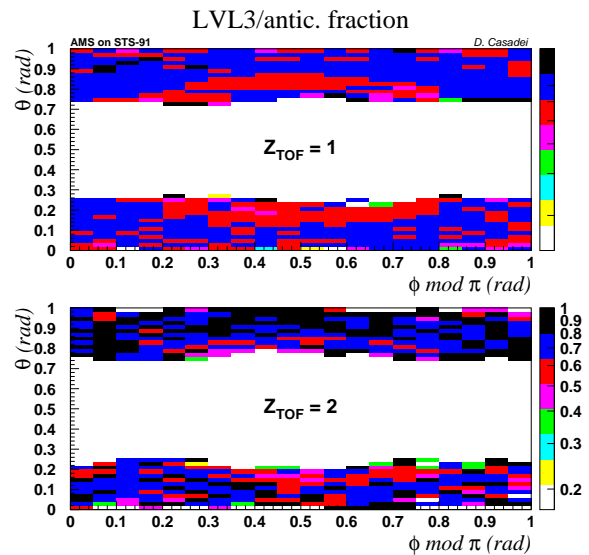


Figure 18. Level 3 to level 1 events ratio as function of direction.

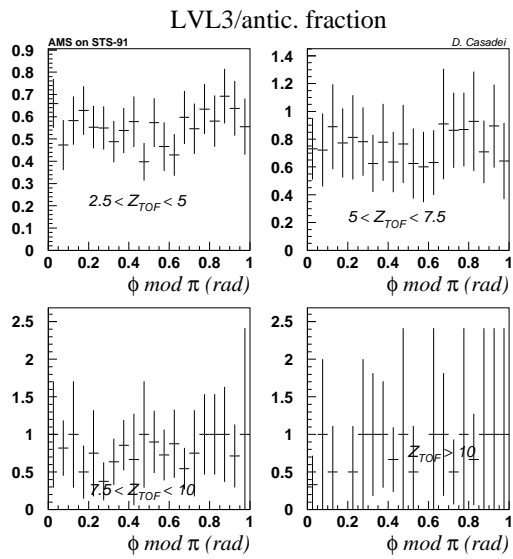


Figure 19. Level 3 to level 1 events ratio as function of direction.

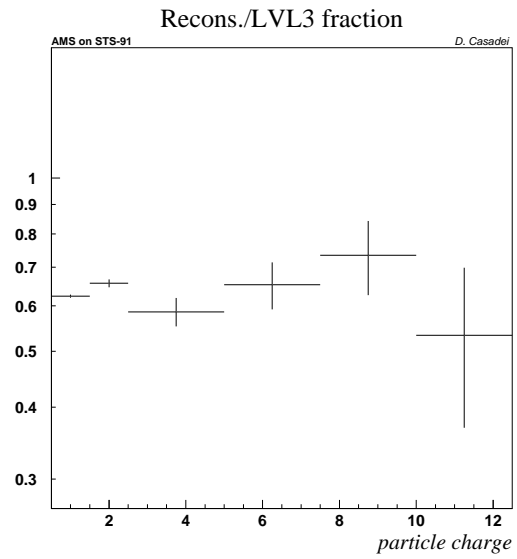


Figure 21. Reconstructed to level 3 events ratio as function of charge.

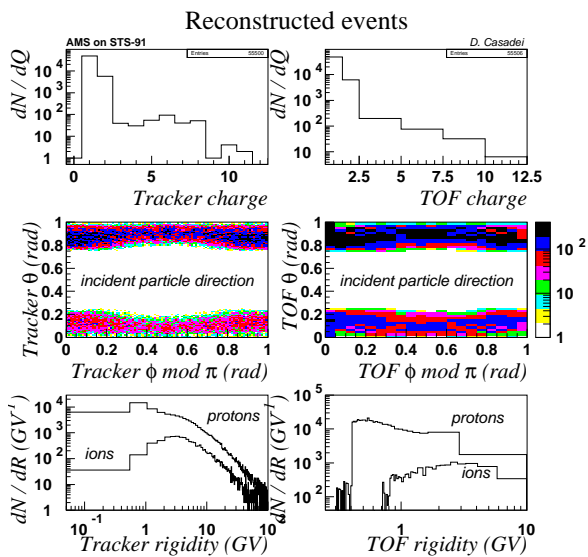


Figure 20. Reconstructed events distribution.

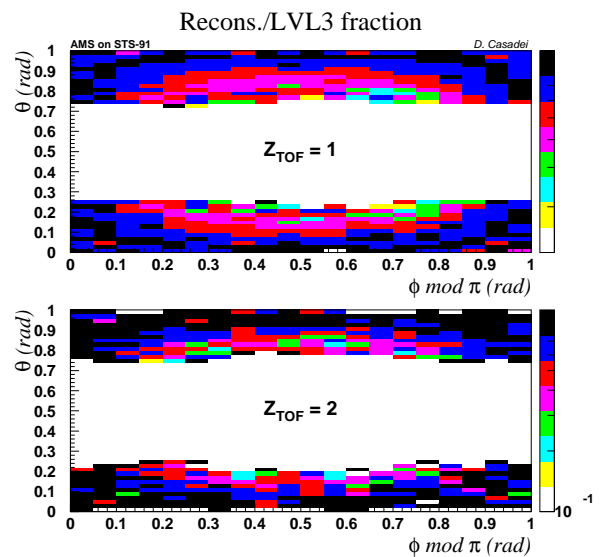


Figure 22. Reconstructed to level 3 events ratio as function of direction.

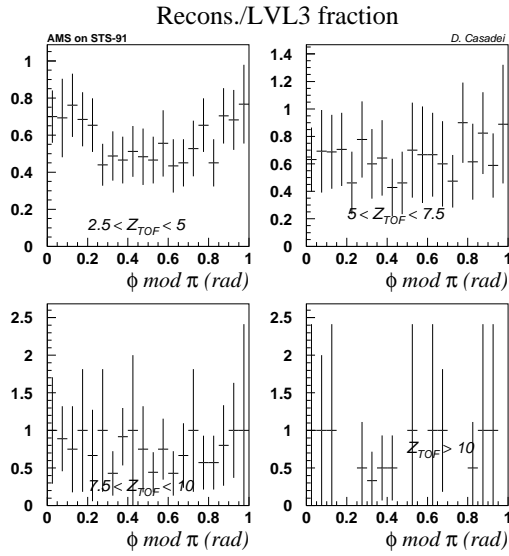


Figure 23. Reconstructed to level 3 events ratio as function of direction.

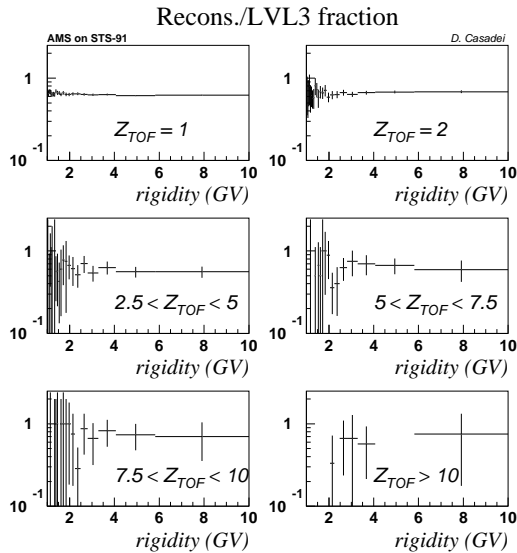


Figure 24. Reconstructed to level 3 events ratio as function of rigidity.

Figures 26, 26 and 27 allow a direct comparison between the different trigger levels rejection power, as function of charge and rigidity.

As shown in figure 26, with respect to He nuclei the protons rejection increases adding more and more trigger conditions, while there isn't any sensible difference for the other ions. In addition, the reconstruction procedure cuts away an additional fraction of high charges (measured by TOF).

Figures 26 and 27 show an increasing rejection for low rigidities.

6. Conclusion

The capability to self-check its efficiency is a invaluable feature of a detector. The STS-91 flight has shown that this feature must be improved for AMS-02, and this has to be done in a twofold manner. Acquiring an event after a given number of “real” triggers seems to be not the optimum: AMS should be able to do this kind of calibration when necessary, simply by switching to the simplest trigger logic and acquiring a sufficient sample of data. The second way is to improve the TOF charge resolution, in order to be able to see how different ions are cut away by the trigger conditions. Incidentally, the presence of a RICH will enlarge the range of rigidity over which a measure can be done.

REFERENCES

- [1] S.P. Ahlen *et al.*, Nuclear Instruments and Methods **A 350** (1994) 351.
- [2] D. Alvisi *et al.*, Nuclear Instruments and Methods **A 437** (1999) 212–221.
- [3] V. Blobel, “Unfolding methods in high-energy physics experiments”, in: Proc. 1984 CERN School of Computing, CERN 85-09 (1985) 88–127.
- [4] D. Casadei, “AMS Time of Flight System Performances During the STS-91 Mission”, AMS-BO Int. Note 2000-03-01 (2000).
- [5] D. Minelli, “Studio dell’efficienza e della stabilità dei contatori a scintillazione di AMS durante il volo sul Discovery” [in italian] thesis work (2000).

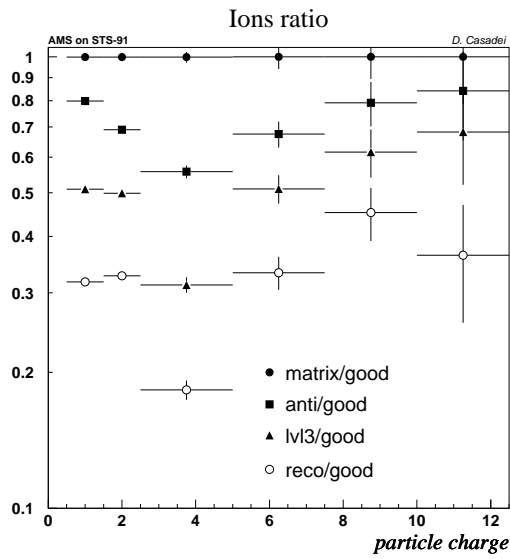


Figure 25. Comparison between different trigger levels rejections, as function of the particle charge.

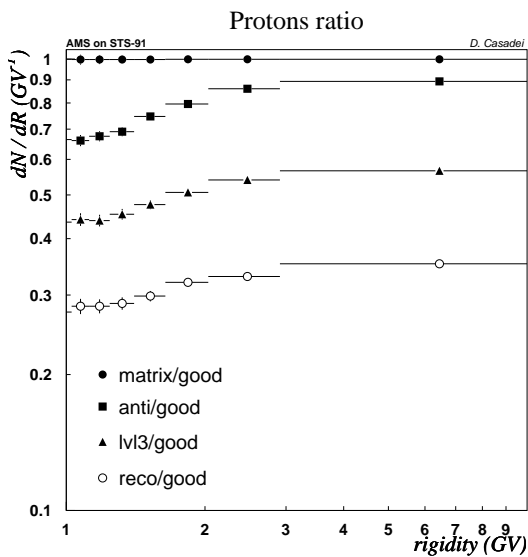


Figure 26. Comparison between different trigger levels rejections, as function of protons rigidity, measured by TOF.

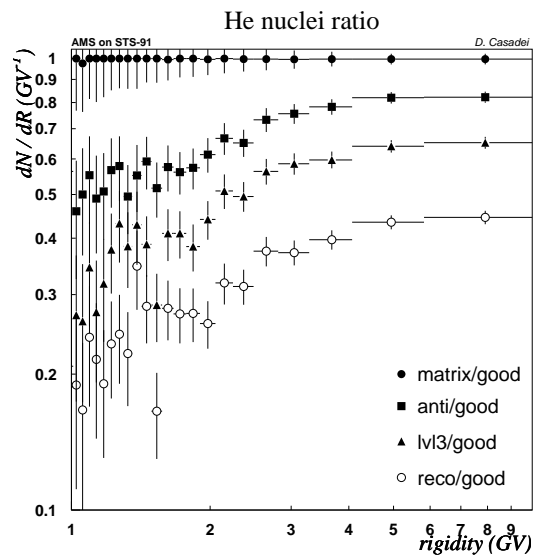


Figure 27. Comparison between different trigger levels rejections, as function of He nuclei rigidity, measured by TOF.